ACS APPLIED MATERIALS & INTERFACES

Research Article

www.acsami.org

Ceramic Pore Channels with Inducted Carbon Nanotubes for Removing Oil from Water

Xinwei Chen,[†] Liang Hong,*[,†,‡] Yanfang Xu,[†] and Zheng Wei Ong[†]

[†]Department of Chemical & Biomolecular Engineering, National University of Singapore, 10 Kent Ridge Cresent, Singapore 119260, Singapore

[‡]Institute of Materials Research and Engineering, 3 Research Link, Singapore 117602, Singapore

ABSTRACT: Water contaminated with tiny oil emulsions is costly and difficult to treat because of the colloidal stability and deformable nature of emulsified oil. This work utilizes carbon nanotubes (CNTs) in macro/mesopore channels of ceramic membrane to remove tiny oil droplets from water. The CNTs were implanted into the porous ceramic channels by means of chemical vapor deposition. Being hydrophobic in nature and possessing an interfacial curvature at nanoscale, CNTs enabled tiny oil emulsion in submicrometer and nano scales to be entrapped while permeating through the CNTs implanted pore channels. Optimizing the growth condition of the CNTs resulted in a uniform distribution of CNT grids, which allowed the development of lipophilic layers during filtration. These lipo-layers drastically enhanced the separation performance. The filtration capability of CNT-ceramic membrane was assessed by the purification of a dilute oil-in-water (o/w) emulsion containing ca. 210 ppm mineral oil 1600 ppm emulsifier, and a trace amount of dye, a proxy polluted water source. The best CNT-tailored ceramic membrane, prepared under the optimized CNT growth condition, claimed 100% oil rejection rate and a permeation flux of 0.6 L m^{-2} min^{-1}, driven by a pressure drop of ca. 1 bar for 3 days on the basis of UV measurement. The CNT-sustained adsorption complements the size-exclusion mechanism in removing soluble oil.

KEYWORDS: *carbon nanotube, porous ceramic, membrane, oil-in-water emulsion, filtration, adsorption*

1. INTRODUCTION

Water pollution has become a major environmental issue because of tremendous growth in industrialization and urbanization. It is widely anticipated that the severity of the problem will escalate in the next few decades with the projected expansion of the world population. One of the major pollutants is oil-in-water emulsion (o/w emulsion), whose sources include the petrochemical industry, petroleum refineries, textile industry, metal industry, domestic sewage, and oil spills.[1] Discharging oily water into water bodies has adverse effects and dire consequences on the environment and human health. The presence of oil is not only aesthetically displeasing; more importantly, it blocks the penetration of sunlight – an essential component of the aquatic cycle. Consequently, this affects the photosynthesis process of aquatic plants and thus reduces the dissolved oxygen level in the water bodies. Furthermore, the gills of aquatic animals can be coated with oil which will hinder their breathing process and eventually lead to death. This will create unnecessary stress on the already depleted supply of the food chain to support the fast growing human population. To date, strict regulations have been imposed in many countries to ensure that oil content in a wastewater stream be reduced to an acceptable level before discharging into water bodies.

Selection of a pertinent purification technique largely depends on the droplet size of oil-in-water (o/w) emulsions. Treatments such as sedimentation,[2,3] flotation,[4−6] and centrifugation treatments work effectively to strip off o/w emulsion particles with sizes greater than 150 μm since these particles are generally immiscible with water. However, the challenge for removing the smaller emulsion particles from water increases dramatically with the decrease in particle sizes, particularly for dealing with those having sizes below 100 nm. In the following sections, the term "dissolved oil" is used to classify those tiny emulsified oil that have particle sizes less than 10 nm and form an o/w microemulsion, i.e. they are clear, stable, isotropic liquid mixtures of oil, water and surfactant. The difficulty is compounded by the deformable nature of oil droplets, which renders the use of size exclusion technique ineffective. On the other hand, biological degradation[7] and activated carbon adsorption[8] are not size-exclusion techniques, which are in general either too costly or inefficient to tackle tiny oil droplets. Such techniques are classified as batch processing, which generally requires large working space and long operation time; all of which will increase the operating cost for the purification process.

As far as membrane separation is concerned, both polymeric and inorganic membranes have been received increasing attention for solving various problems of water treatment because of their higher energy efficiencies, lower cost and compact designs compared to the nonfiltration methods. In the application of polymeric membranes, both ultrafiltration (UF)[9−11] and microfiltration (MF)[12] have proven to be effective in desalination. Nevertheless, accumulation of fouling on the membranes requires regular cleaning by either rigorous backwashing or chemical treatment in order to restore the membranes performance.[13,14] This auxiliary treatment also makes the polymeric membranes unpractical for removing emulsion from water because the polymeric membrane materials are normally vulnerable to organic solvents and heat treatment, which will cause changes in pore

Received: October 4, 2011
Accepted: March 20, 2012
Published: March 20, 2012

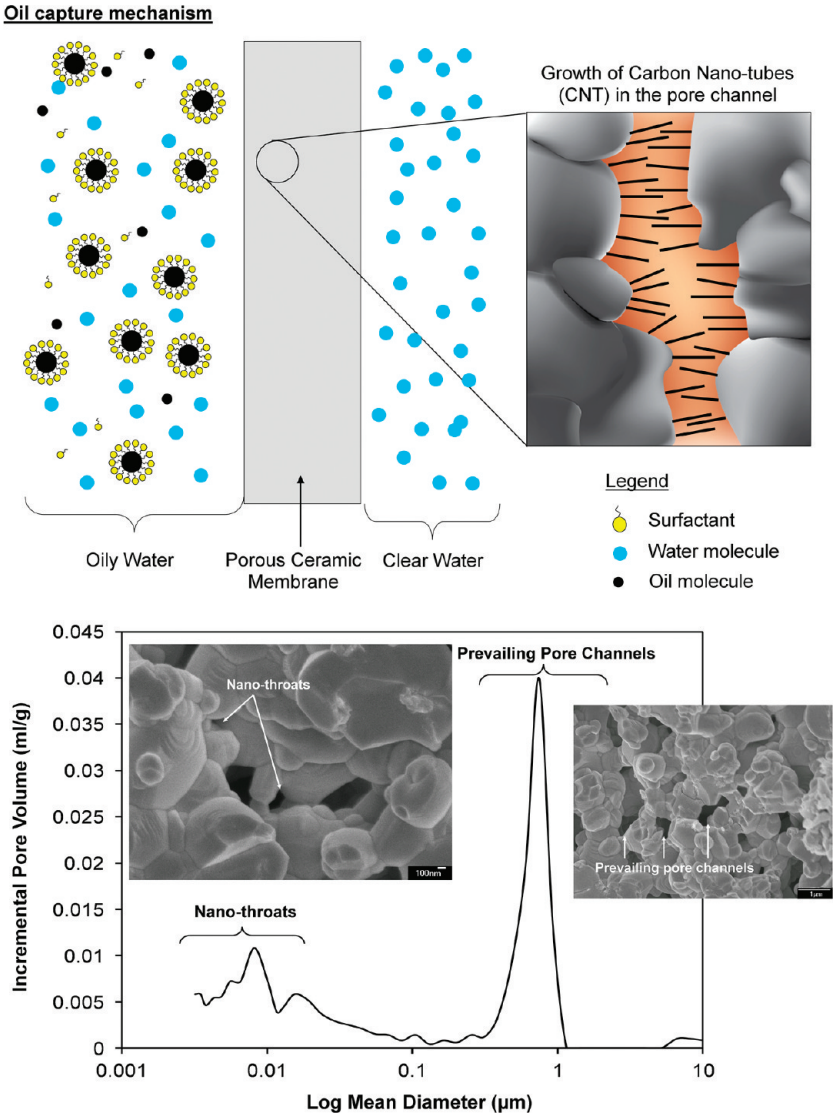

Figure 1. Ideology of oil capture mechanism by carbon nanotubes grown in pore channels of a porous ceramic membrane. The pore size distribution of the porous ceramic membrane used is determined by mercury porosimetry. FESEM micrographs confirm the occurrence of nanothroats and prevailing submicrometer pore channels in the disk.

structures. In contrast to the polymeric membranes, the porous inorganic membranes possess obviously superior antifouling capability besides their stronger chemical, thermal and mechanical stabilities.[15,16] These properties ensure long operation life, which translates to a more cost-effective means after factoring in the material and fabrication costs. As such, there is a growing interesting in using inorganic membranes for purifying oil-contaminated water in recent years.[14] However, as aforementioned, the limitation to filtering out small oil droplets from water by the size-exclusion technique remains.

Assimilation of adsorption sites into size-exclusion membrane channels would be an effective way to treat dilute o/w emulsions. Hence, we proposed the idea of implanting carbon nanotubes (CNTs) in the pore channels of a ceramic membrane to form nanogrids for capturing smaller oil particles (<500 nm) (Figure 1). Fundamentally, CNTs endow hydrophobic affinity through the CH/π-interactions[17] and are adequate adsorption sites for oil molecules in water.[18−21] Two latest developments which involved incorporating CNTs into the surface of a polymer membrane for oil/water separation[20] and growing vertically aligned CNTs on stainless steel (SS) mesh for purifying oily water[21] made use of the lipophilic nature of CNTs. The superhydrophobic and superoleophilic properties of CNTs have also been employed for water/oil purification, where the repulsion to water molecules allowed only oil to permeate through the membrane.[22,23] Furthermore, CNT possesses stout tensile strength and Young's modulus that are 10−20 times and 5 times greater than stainless steel, respectively.[24,25] This permits CNTs to withstand vigorous shear flow during filtration. Hence, the integration of CNTs with porous ceramic membranes would explore a niche application of CNTs.[26]

In this work, CNT grids were implanted in the porous ceramic membrane through chemical vapor decomposition of methane inside the pores, which was catalyzed by the nickel nanodomains distributed uniformly over the pore channels. The porous ceramic was prepared by the in situ pore-forming approach,[27] which created a hierarchical pore-size system involving two pore dimensions in the resultant porous ceramic membrane (Figure 1). The larger pore group allowed only oil particles smaller than 1 μm and the dissolved oil to enter the pore

channels through the ceramic membrane while the smaller group increased the inherent flux and strengthened the mechanical properties of the ceramic membrane. This size-exclusion feature ensured that the primary functionality of the implemented CNT grids is to block the tiny emulsion particles. The continuous adsorption of oil with filtration resulted in formation of an oily (or lipophilic) layer on the CNT grids primarily and this lipo-layer subsequently facilitated seizure of oil particles. The synergy of the size exclusion and hydrophobic adsorption renders the membrane effective to purify substantially diluted and stable o/w emulsions.

2. MATERIALS AND METHODS

2.1. Preparation of the CNT-Tailored Ceramic Membrane. Porous disk of yttria-stabilized zirconia (YSZ) in cylindrical shape ($d \times t$ = 2.6 × 0.19 cm) was fabricated using the in situ pore-forming technique as disclosed elsewhere.[27] The YSZ disk has an approximate volume-based specific surface area of 22 m^2/cm^3 and a porosity of 36%. The pore size distribution of the membrane is shown in Figure 1, where the majority of the pores lie in between 0.7 and 1.0 μm and are connected by a portion of throat pores (<50 nm). The ceramic membrane was submerged in a nickel nitrate ethanol solution (5.47×10^{-4} to 24.6×10^{-4} M) and sonicated for 15 min. The membrane was then removed and dried in an oven at 80 °C for another 15 min, leaving behind uniformly distributed tiny nickel nitrate particles inside the pores of the YSZ membrane. This step was repeated thrice to ensure all the pores were loaded.

The nickel nitrate loaded porous YSZ membrane was purged with H_2 for 5 min in a quartz tube (internal diameter of 31 mm) at room temperature, which was followed by heating the tube to and held at 400 °C for 1 h under a hydrogen stream (16 L/h) to allow for formation of Ni(0) nanodomains through in situ reduction. The temperature was then raised to a designated temperature in the range from 400 to 800 °C by a heating rate of 15 °C/min without swapping the H_2 atmosphere. Subsequently, the inlet was switched to a pure methane stream (8 L/h) and the methane undertook thermal cracking on the freshly generated Ni(0) domains, leading to in situ growth of CNTs. After 1 h of reaction, the purging stream was switched back to H_2 and the reactor was cooled down to room temperature. To specify the preparation history of a sample, the symbol YSZ-CNTs (× °C, × M) is used to denote the membrane in the following parts, where the first alphabet in the bracket represents the CNT growing temperature and the second number the concentration of impregnation solution: $Ni(NO_3)_2$-g/ethanol-ml.

2.2. Microscopic and Surface Area Examinations of the CNT-Tailored Ceramic Membranes. The cross-section images of the membranes were obtained from field-emission scanning electron microscope (FESEM, JEOL JSM-6700F, Tokyo, Japan). Prior to this, the samples were coated with a thin layer of platinum to prevent electron accumulation during observation.

The morphology of the in situ grown carbon nanotubes was examined under Transmission Electron Microscope (TEM, JEOL JEM-2100F, Tokyo, Japan). A small piece of CNT-ceramic membrane was grinded and the resultant fine powder was dispersed in ethanol. The mixture was then ultrasonicated for 10 min and left to stand for another 10 min. A drop of the top liquid layer containing the dispersed CNTs was transferred to a copper grid and followed by drying. The residue on the grid was then examined by TEM.

The total surface area of the CNTs in the ceramic membranes were derived from the adsorption isotherm curve of N_2, which was measured using Pore and Surface Analyzer (Autosorb-1c, Quantachrome Instruments, Florida, USA). Multipoint Brunauer, Emmett and Teller (BET) method was used for this purpose. Prior to all measurements, the samples were degassed at 300 °C for 3 h.

2.3. Preparation and Quantification of O/W Emulsion. The o/w emulsion was prepared as follows: 150 μL of blue ink (69% of mineral oil, Metal Ink, Lion, Japan) and 0.8 g of sodium dodecyl sulfate (SDS, Fluka, Switzerland) used as emulsifier were added to 500 mL Millipore water. A stable o/w emulsion containing ca. 210 ppm oil and 1600 ppm emulsifier was generated after consecutive mechanical mixing and ultrasonication for a day. The blue ink provides a visual inspection of the water quality of the filtrate during filtration. The particles' size were determined by dynamic light scattering (90 Plus, Brookhaven Instruments Corporation, New York, US) and observed under microscope.

The concentration of o/w emulsion particles in water after filtration, namely filtrate, was determined by UV spectroscopy (UV-3600, Shimadzu, Singapore). Prior to the measurement, a calibration curve was plotted using a group of o/w emulsions prepared by diluting the above o/w emulsion with water in different proportions. By applying the Beer–Lambert law the absorbance of the diluted o/w emulsions is linearly proportional to their concentration. It may be noted that the UV spectroscopy measurement is based on the λ_{max} of blue dye dissolved in oil droplets of emulsion. Hence this analytical method has its own limitation to detect the dissolved oil, i.e., microemulsified oil, as defined above. Thus to quantify the concentration of the dissolved oil, the analysis was carried out on an oil content analyzer (OCMA-300, Horiba, Singapore). One ml filtrate sample was mechanically mixed with 19 mL of Millipore water and 10 mL of a specific solvent (S-316, Horiba). The mixture was then settled for 200 s to allow complete separation of 2 liquid layers after the extraction treatment. The bottom aqueous layer which only contains the dissolved oil was sent to the analyzer for measurement.

2.4. Permeation Measurements and Restoring Performance of Spent Membrane. A filtration membrane test kit was designed (Figure 2), which comprised of a gear pump, a valve, and a pressure gauge. The effective membrane area used for permeation measurements was 3.142 cm^2 and the filtration was conducted at 25 °C. The trans-membrane pressure was kept at 1 atm. The reservoir contains the feed (o/w emulsion) as prepared in Section 2.3. The permeation flux (PF) was calculated by formula 1, where the volume of permeate (V, cm^3), membrane area (A, cm^2), and time (t, s) were measured.

$$PF = \left(\frac{V}{At}\right) \tag{1}$$

Rejection (R), calculated on the basis of the UV spectroscopy measurement, was as follows

$$R(\%) = \left(1 - \frac{C_p}{C_f}\right)100 \tag{2}$$

where C_p represents concentration of a particular component and C_f is its feed concentration. It is worth noting that the dissolved oil concentration was determined by the oil content analyzer and was not used for the calculation of the rejection. A dry run was conducted to ensure that no CNTs were unbound from pore channels under the shear stress of water, the selected permeated water samples were examined by TEM and no any single CNT was found.

After being used in filtration for 3 days, the YSZ-CNTs (750 °C) membrane was regenerated by placing it in a reflux system which was operated at 130 °C for a day with toluene as the solvent for the oil. The regenerated membrane was then dried in oven at 50 °C. It was confirmed by electron microscopy that the CNTs were free of grease and ready for reuse.

3. RESULTS AND DISCUSSION

3.1. Growth of CNTs in YSZ Membrane. CNTs were grown in the pore channels of YSZ through thermal cracking of methane on Ni(0) domains distributed whereby beforehand. It has been known that CNTs are normally grown on a flat planar support[28] and few studies have explored the growth of CNTs on a concave and/or rough surface. One of these attempts has grown CNTs in the straight pore channels of alumina substrate,[29] which has a different pore structure from the porous YSZ substrate used in this work. The YSZ substrate is dominated by 3D interconnected submicron pore channels with a spread of

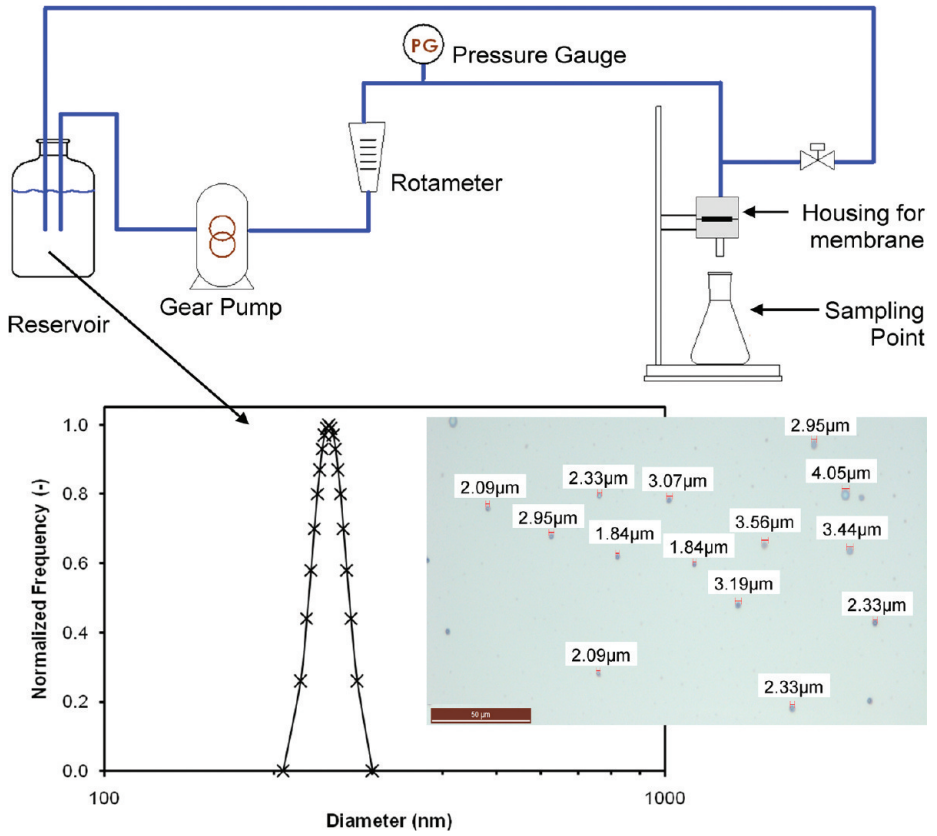

Figure 2. Schematic of membrane filtration system. The feed of the reservoir contains surfactant stabilized oil-in-water emulsion with the majority of the particles' size falling in the range of 210 and 300 nm determined by dynamic light scattering. The average particle's diameter is 250.9 nm. (Inset) Emulsified oil particles in water observed under microscope with sizes ranging from 2 to 4 μm. However, these were not detected by the dynamic light scattering.

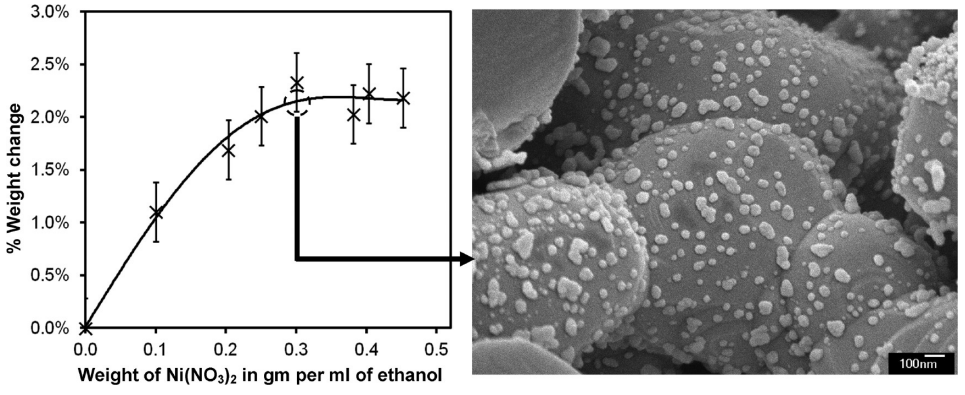

Figure 3. Variation in Ni(0) particle loading inside the YSZ membrane with the increase in concentration of $Ni(NO_3)_2$ alcohol solution. A cross-section FESEM micrograph shows a uniform spread of Ni(0) domains through YSZ pore channels after H_2 reduction.

nano percolation throats throughout these pore-channels as demonstrated in Figure 1. Hence, the challenge lies in whether an even distribution of Ni(0) domains could be achieved over the narrow and tortuous pores channels for the growth of CNTs. This problem was tackled by using ethanol as the solvent for nickel nitrate (the precursor for Ni(0) catalyst) instead of water primarily because ethanol offers a lower surface tension. In addition, ultrasonication was applied to enhance penetration of the solution into the pore channels as the ability of ultrasound waves to induce acoustic cavitation in the bulk of liquid facilitated the infiltration of fluid into those tiny pores.[30]

Figure 3 displays the relation between the concentration of nickel nitrate in ethanol and the loading of Ni nanoparticles in the YSZ eventually obtained. The loading of Ni(0) in YSZ increased with increasing concentration of nickel nitrate in ethanol and reached a plateau when the concentration was 0.3 g/mL and higher. This turning point was then taken as the upper-boundary concentration for the preparation of catalyst. Using the aforementioned deposition strategy we attained the desired result according to FESEM observation, which shows a uniform distribution of Ni(0) domains with sizes ranging from 5−50 nm on the pore walls according to an arbitrary cross section of the membrane.

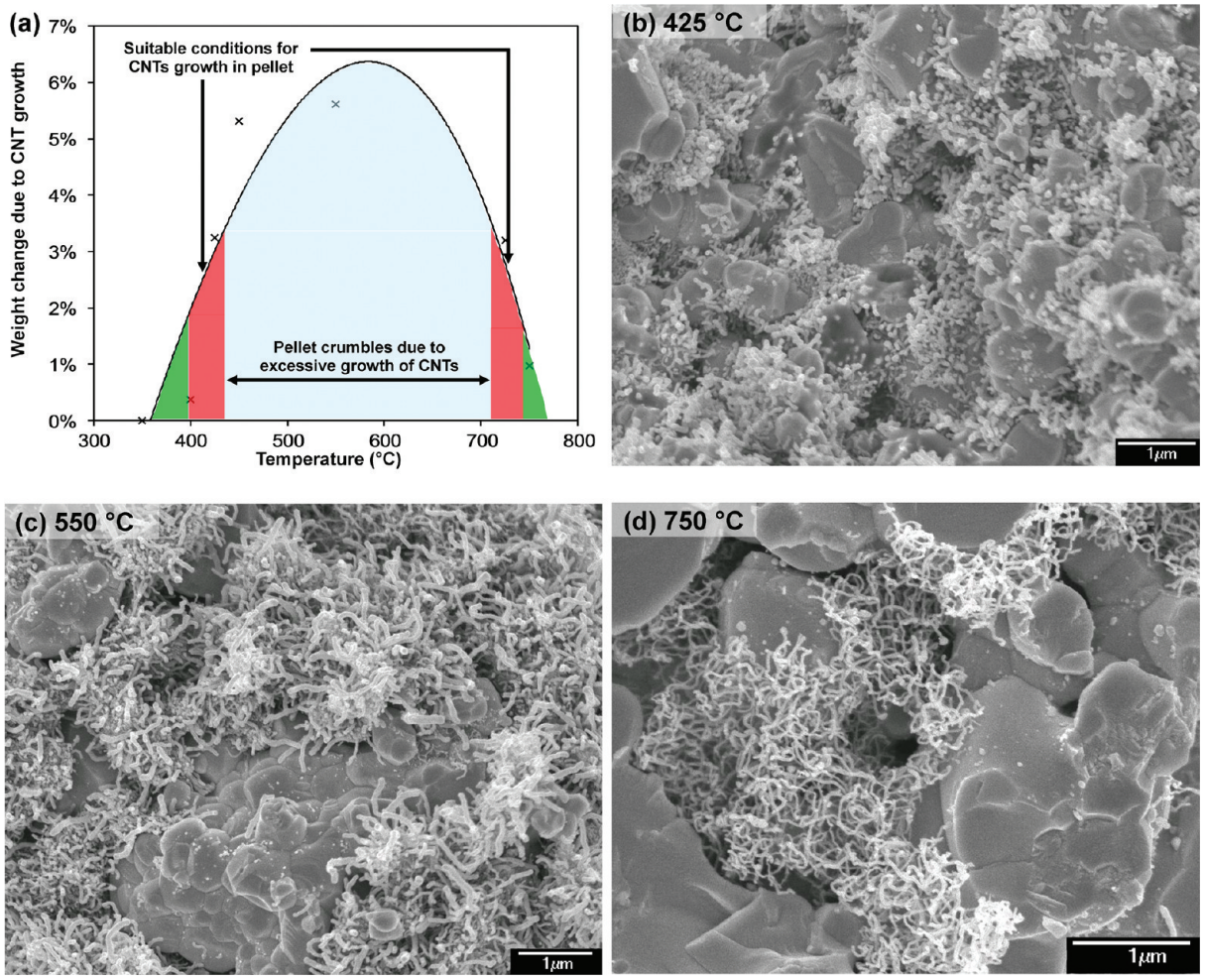

Figure 4. (a) Growth of CNTs in the Ni(0)-loaded YSZ membranes based on the use of $Ni(NO_3)_2$ ethanol solution (0.3 g/mL). The light blue (425 °C < T < 725 °C) region in the CNT wt %−T chart represents excessive growth of CNT, which led to crumbling of membrane, whereas little or no CNT growth happened in the regions labeled by green (T < 400 °C or T > 725 °C). (b−d) FESEM micrographs of the cross sections of YSZ membrane, in which the growth of CNTs was conducted at various temperatures as specified.

Figure 4 displays the crucial effect of the temperature at which the thermal cracking of methane was conducted on the growth of CNTs in the Ni(0)-loaded YSZ membranes. Generally, a temperature higher than 700 °C causes a significant decrease in the amount of CNTs because of the deactivation of the nickel catalyst. An independent study has reported that the Ni(0) catalyst presents a maximum activity for carbonization of CH_4 at about 650 °C.[31] Indeed, an exorbitant growth of CNTs occurs at temperatures higher than 425 °C, which consequently causes the membrane to crumple due to the tension built up inside the pore channels. Hence, it was concluded that there exist suitable processing conditions with regards to the Ni(0) loading and the methane thermal cracking temperature for achieving a dense and uniform CNTs loading. The FESEM images taken from the cross sections of the three CNTs-YSZ membranes reveal randomly entangled CNTs grown in pore channels (Figure 4). It was observed that the CNTs grown at 425 °C are much shorter despite being more concentrated and highly spread than those grown at 750 °C. It is clear that CNTs grown at the higher temperatures formed sponge-like grids that are required for effectively capturing oil particles. The structural characteristic of sponge-like grid can be more clearly verified by examining a small grain taken from the membrane (750 °C) after it was crushed (Figure 5). A nanosized nickel particle was found at near the top end of a CNT, indicating that the growth of CNT is by tip mode.[28] In addition, the CNTs are multiwalled with parallel well-graphitized walls and are hydrophobic in nature. It is interesting to know the surface area provided by these CNTs. The BET analysis of the pristine YSZ showed a too low surface area that can be determined by using N_2 as adsorbent. On this substrate, the CNTs grown at 425 °C (Figure 4) increased the surface area to 4.0 m^2/g, reflecting the contribution of the short and concentrated CNT "roots", whereas the CNT grids grown at 750 °C offered instead a bit lower surface area of 2.4 m^2/g. This result describes the fact that CNTs possess dense surface.

3.2. Removal of Oil from O/W Emulsions by the CNTs-Tailored YSZ Membrane. As the key performance indexes of a separation membrane, the rejection and permeation flux of the four CNTs-YSZ membranes were assessed in Figures 6 and 7. It should be noted that the rejection in Figure 6 was obtained from the UV measurement. For the growth of CNTs at 750 °C, the use of 0.3 M $Ni(NO_3)_2$/alc. as impregnation solution resulted in small defects along the edge of the ceramic due to abundance growth of CNTs. This preparation condition was therefore abandoned. According to these two figures, the implantation of CNT grids in the pore channels clearly improved the rejection performance in comparison with the

dx.doi.org/10.1021/am300207b | ACS Appl. Mater. Interfaces 2012, 4, 1909−1918

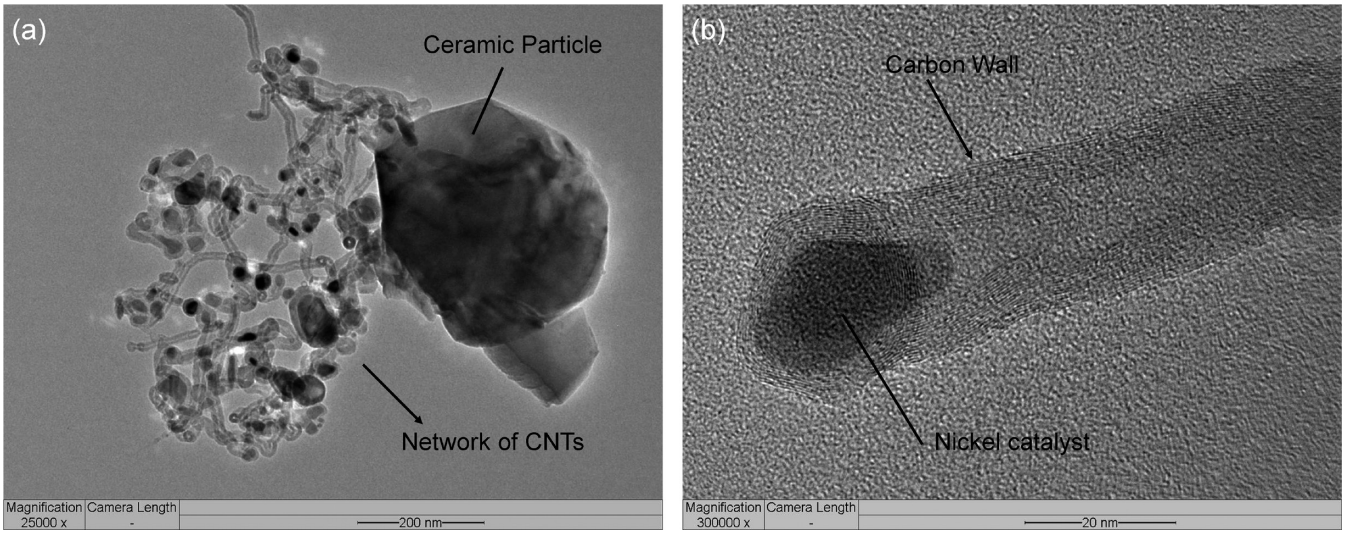

Figure 5. TEM micrographs: (a) network of CNTs formed surrounding a ceramic particle, (b) close-up view of a single strand of CNT.

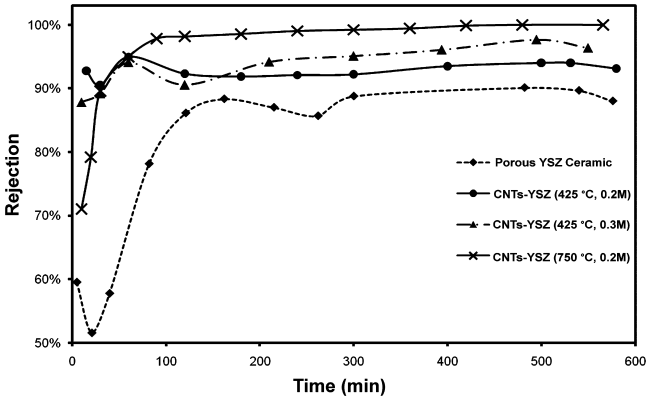

Figure 6. Variations in rejection to oil of an o/w emulsion of a membrane with the time of separation: (♦) porous YSZ ceramic membrane, (●) CNTs-YSZ (425 °C, 0.2M), (▲) CNTs-YSZ (425 °C, 0.2M), and (×) CNTs-YSZ (750 °C, 0.2M) (see section 2.1 for the sample ID).

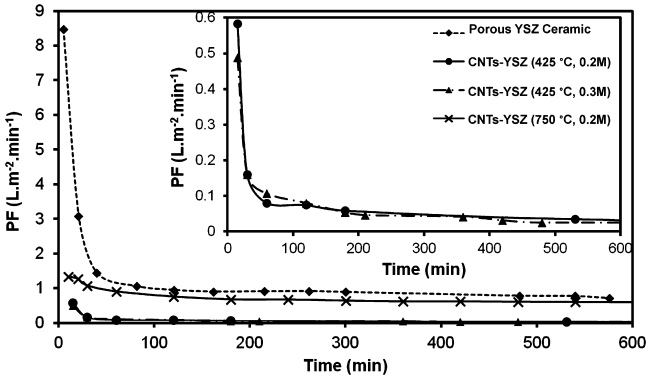

Figure 7. Variations in permeation flux of a membrane with the time of separation: (♦) porous YSZ ceramic membrane, (●) CNTs-YSZ (425 °C, 0.2M), (▲) CNTs-YSZ (425 °C, 0.3M), and (×) CNTs-YSZ (750 °C, 0.2M).

pristine YSZ membrane. The steep rejection rate profile exhibited by either the pristine YSZ membrane or the CNT-YSZ (750 °C, 0.2M) membrane in the first 100 min separation duration indicates the development of a soft layer due to adsorption of emulsion particles onto the pore channels. In particular, in the CNT-YSZ (750 °C, 0.2M) membrane, the CNT grids functioned like a "wave breaker" to increase the interfacial contact time of emulsion particles and hence facilitated the adsorption. As to the two CNT-YSZ (425 °C) membranes studied, an instantaneous development of such a soft layer must have occurred immediately after the start of filtration because of the higher rejection rate than what happened in CNT-YSZ (750 °C) in the very initial stage of separation. It can be attributed to the fact that these two membranes possessed higher surface coverage of short CNT wedges in their pore channels as supported by Figure 4. Thereby the densely spread CNT wedges grafted the emulsion particles swiftly. The rejection curves of the pristine YSZ and the CNTs-YSZ (425 °C, 0.3M) membranes each exhibited a small concave shape after reaching their maximum values. This phenomenon is likely caused by the detachment of the adsorbed grease layer at a few locations under the action of shear flow. The curve of CNTs-YSZ (750 °C) membrane did not exhibit such random variation because of effective filtration by CNT grids. The separation reached a steady state after approximately 100 min, which suggests the establishment of equilibrium between the shear flow and emulsion adsorption. After that, the soft layer changed its role from principally trapping down emulsion particles to rejecting them when it became thicker because of the narrowing of flow passage. It may noteworthy that the rejection mentioned here is about those emulsion particles smaller than the rigid membrane pore sizes. This soft-reject-soft interaction between the grease layer surface and colloids is sustained by the osmotic pressure caused by the lower fugacity of water film sandwiched in between the surface and colloidal particles than the water surrounding it.[32] Indeed, both YSZ and CNTs-YSZ (750 °C, 0.2M) membranes displayed comparable permeation flux pattern after 100 min separation (Figure 7), implying that the resistances to flow due to the no-slip layer effect in them were similar. However, the latter membrane manifested the highest level of oil rejection in contrast to the former membrane (Figure 6). It is deemed that the CNTs grids gave rise to a far greater number of narrower channels in contrast to the pristine YSZ passages. It was each of these numerous narrower channels with CNT grids that contributed to steric exclusion of the tiny emulsion particles due to the presence of fugacity gradient as aforementioned.

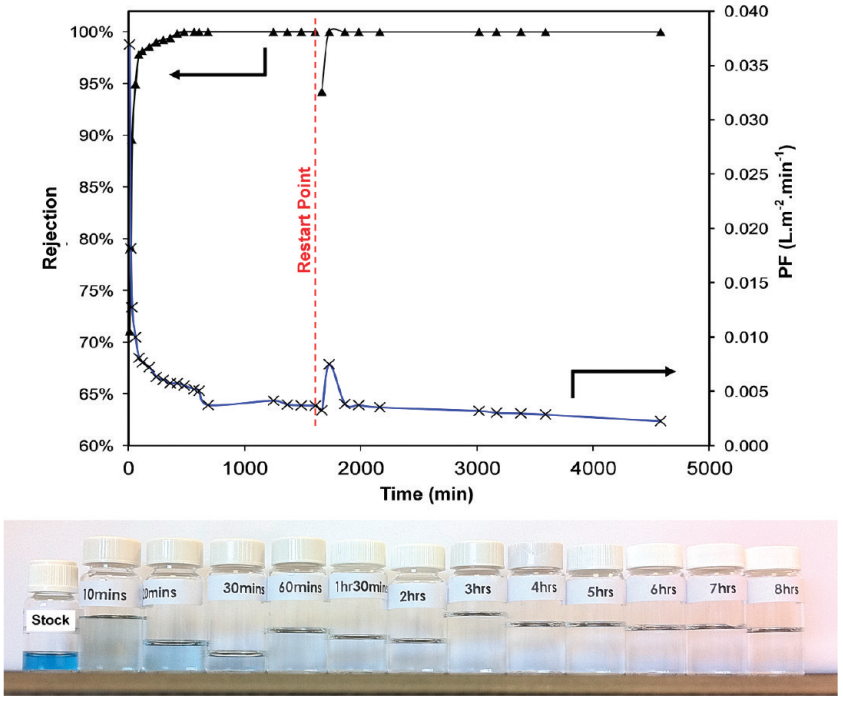

Figure 8. Examination of the performance of the CNT-YSZ (750 °C, 0.2M) membrane over a period of 3 days. (Inset) Filtrated water samples collected at various timing during the filtration process.

Another corresponding observation in relation to the formation of an oily soft layer in the pore channels is the large decrease in permeation flux (Figure 7). As expected, the pristine YSZ membrane showed the least decrease in flux among the four membranes because it displayed the lowest rejection rate profile due to limited spatial extension of the soft layer. In contrast to the pristine YSZ membrane, both CNT-YSZ (425 °C, 0.2 and 0.3M) membranes gave substantially lower fluxes. This can be interpreted as the plugging of the pore channels by the oily soft materials originated from the densely spread short CNT wedges as addressed above. It is also worth noting that despite a very low flux, the oil rejection rates of these two membranes were still well below 100%, which represents the adsorption equilibrium on the lipo soft layer supported by short CNTs. Shifting our focus to the CNT-YSZ (750 °C, 0.2M) membrane, the CNT grids were protruding and evenly distributed throughout the pore channels as shown in Figures 4 and 5. The extrusion of tiny droplets of oil was prevented because the grease layer was developed on CNT grids rather than in the narrow constricted area in the pore channel of the ceramic membrane. The stretching of CNT grids prevented the pore channels from being plugged by the lipo soft materials. More importantly, the adsorption equilibrium on the lipo soft layer deposited on CNT grids possesses insignificant desorption tendency. Finally, the performance durability of CNT-YSZ (750 °C, 0.2M) membrane was examined over a three-day period (Figure 8) and it was observed that the oil rejection and permeation flux profiles showed negligible difference from those presented in Figure 6.

As indicated in Figure 1, the pore channels in the pristine YSZ membrane possessed two typical pore widths; therefore, size-exclusion was not the only separation mechanism. To a certain extent, the extrusion mechanisms prevailed in the separation process before steady state was reached. A portion of oil droplets in the o/w emulsion were softer and bigger than the pore widths available. Hence, the extrusion of emulsion particles, driven by trans-membrane pressure of 1 atm, took place particularly in the throat pores as defined above. The extrusion also promoted adsorption of oil concurrently because the shearing stress helps to remove the emulsifier from emulsion particles. The adsorption subsequently lead to a lipophilic soft layer comprising oil and surfactant molecules in pore channels, which in turn acts as a natural filtration barrier for trapping big oil droplets initially and subsequently rejecting them.[12]

3.3. Enhancing Size-Exclusion Separation Selectivity by Implementing CNT Grids. Implantation of CNTs grids in the pore channels of YSZ membrane effectively augmented the capability of developing lipophilic grease layers in the pore channels through the halting of passage of the emulsion particles. Figure 9 displays the development of the grease layer on CNT grids starting from the feed side. On the basis of FESEM images, bridging among different lipophilic grease layers on CNTs resulted in a web in which the pores allow only pure water to slip through. Smaller droplets of oil were either captured by the grease web or blocked and then merged together. Hence, the size-exclusion mechanism can be attributed as the primary separation mechanism after the steady state was established. This explanation is supported by the nil presence of the emulsified oil content in the filtrate from CNTs-YSZ (750 °C, 0.2M) membrane.

As defined above, the dissolved oil, existing in the form of microemulsion, represents the smallest portion of o/w emulsion and is also the most difficult to separate. It has been described in the experimental section that this portion of oil was analyzed by the Horiba oil-content analyzer and the results of the filtrate was shown in Figure 10. As underlined above, the larger emulsified oil droplets were analyzed by the UV spectroscopy method as presented in Figure 6, whereas the content of the dissolved (or microemulsified) oil in a filtrate was solely determined using the oil-content analyzer that has a detection limit to lower concentrations. Applying the latter detection approach, no dissolved oil was found in the filtrate through the CNTs-YSZ (750 °C, 0.2M) membrane in the initial 350 min (Figure 10).

dx.doi.org/10.1021/am300207b | ACS Appl. Mater. Interfaces 2012, 4, 1909−1918

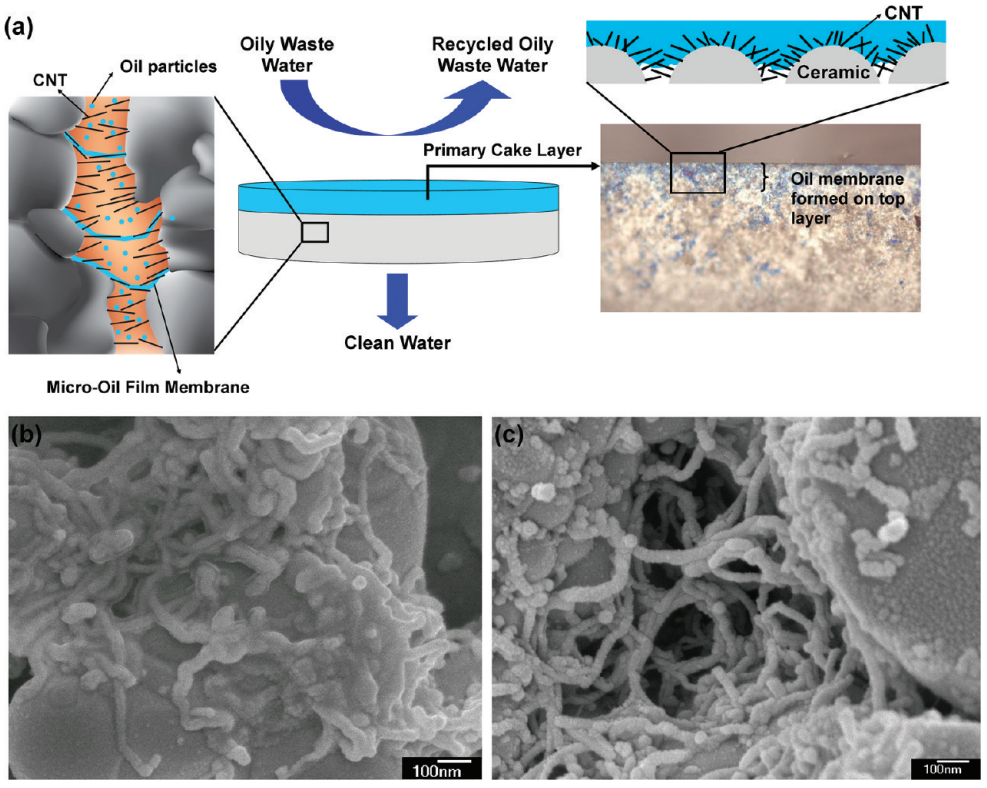

Figure 9. (a) Schematic illustration is incorporated to elucidate the mechanism of forming the grease layer on the surface of the membrane and the action of CNTs during the course of filtration. Microscopic examination on the CNTs-YSZ (750 °C, 0.2M) membrane after filtration was included. (b) FESEM images of the cross-section of the membrane after filtration showing the oil-covered CNTs. (c) FESEM image of the cross-section of the membrane after regeneration showing that the coated oil was removed.

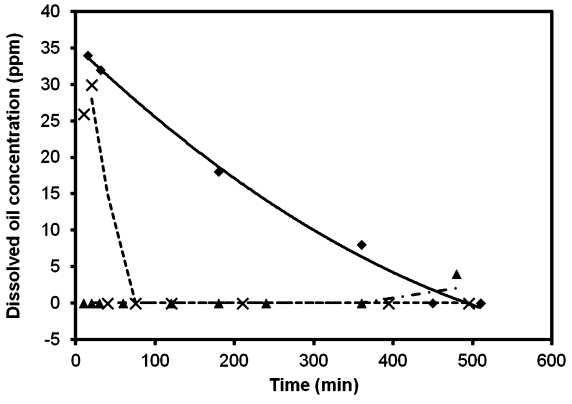

Figure 10. Concentration of dissolved oil in the filtrate through various membranes: (♦) pristine YSZ, (×) CNTs-YSZ (425 °C, 0.3M) membrane, (▲) CNTs-YSZ (750 °C, 0.2M) membrane. The first number in the bracket represents the temperature in which the CNTs were grown, whereas the second number represents the concentration of nickel nitrate solution in ethanol.

There was however a few ppm of dissolved oil permeating the membrane after 350 min. This slight turning-on outcome could be attributed to adsorption/desorption equilibrium as afore-described, which would shift to desorption side when the piling of the grease layer reached a certain thickness in the intricate fluid field. This desorption-caused leak involved only soluble oil and hence was not reflected in the 100% oil rejection determined by UV spectroscopy measurement as displayed in Figure 6, which had remained unchanged over the entire process of filtration of 3 days.

On the contrary, both pristine and CNTs-YSZ (425 °C) membranes showed infiltration of microemulsion with a decreasing trend in the initial stage (Figure 10). The former membrane required an apparently longer time to tight up the permeation of microemulsion than the latter membrane. This is the rational outcome because CNTs in the latter membrane assisted more effectively with capturing the microemulsion particles than just the blank pore channels in YSZ. Similar to the above elucidation regarding the CNTs-YSZ (750 °C) membrane, while none of the dissolved oil was detected from the filtrate through CNTs-YSZ (425 °C) membrane, a certain amount of larger emulsion particles could still be found. This observation has been attributed, in the preceding discussion, to desorption and subsequently aggregation of oil molecules from the lipo-layer. The root cause was that the CNTs in this membrane were too short to effectively withhold the overlying lipo-layer during filtration; hence the observed 2−3% oil penetration throughout the whole filtration course existed.

The recently reported membranes for treating dilute o/w emulsions are compared with the present membrane in Table 1. With reference to the inorganic membranes, the CNTs-YSZ (725 °C) membrane outperformed in terms of rejection performance and duration of operation. It is important to note that most of the membranes in literature were still unable to handle soluble oil because of the deformable nature and tiny phase sizes of this component, leading to rejection rate below 100%. This highlights the role of CNTs in assisting the removal of the tiny oil droplets or dissolved oil. Moreover, the spent CNTs-YSZ (725 °C) membrane can be refreshed through solvothermal treatment in a reflux of toluene. The cleaned membrane showed grease-free CNT grids (Figure 9c).

Table 1. Comparison with Literature Data[a]

membrane				feed condition				performance			
material	pore size (μm)	thickness (mm)	configuration	type of oil emulsion	C_f (mg/L)	CFV (m/s)	TMP (bar)	normalized flux (L m^{-2} h^{-1} bar^{-1})	R^d (%)	duration (min)	ref
YSZ with CNT	0.7 (dominant pore)	2	pellet	blue oil based ink with SDS as surfactant	210	0.005	1	36	100	4320 (3 days)	this work
NaA zeolite coated α-Al_2O_3	1.2	3	tubular	lubricant oil with surfactants: polyoxyethylene (80) sorbitan monooleate	100	0.003	0.5	36	98.8	600	14
α-Al_2O_3	0.5		tubular	edible oil	500	1.68	1	63.9	98.1	70	33
mullite-alumina	0.3	5	tubular	C8−C12 with Triton X-100	1000	1.5	3	20.2	94	120	12
glass	0.27	2	tubular	mineral oil with Tween 85	1 mL/L	0.13	0.68	1.2×10^6	60−98	120	34
ZrO_2- α-Al_2O_3	0.2		tubular	*p*-xylene with fire fighting foam	3000	4.5	1	400	96	170	35
polyamide/ polysulfone support			spiral-wound	from local factory	170	0.009	4	5	99.7	120	36
cellulose membrane			flat sheet	soybean oil	5000		4	1100	97.54	2400	37

[a]TMP = trans-membrane pressure, CFV = cross-flow velocity, C_f = oil concentration of feed, C_p = oil concentration of a particular component, R^d = oil rejection coefficient.

The rejection capability of the membrane is assumed due to the increase in surface roughness of the CNTs. This in effect will promote the ability to trap oil particles and fasten the formation of the lipo-layer, which is beneficial to removing the smaller oil particles in the water stream. This post treatment also demonstrates the advantage of the chemical resistance the CNTs-YSZ membranes possess, which is usually not for polymeric membranes.

4. CONCLUSIONS

A conceptual design of membrane through integration of nanotechnology and traditional ceramic membrane for purification of oil-in-water (o/w) emulsion has been attempted. Carbon nanotubes (CNTs) were grown in pore channels of an Y_2O_3−ZrO_2 (YSZ) membrane by chemical vapor deposition, whereby a uniform distribution of nickel(0) nanodomains, serving as catalytic sites for the growth of CNTs, has been attained. A maximum loading of nickel catalyst particles was determined and two specific methane-cracking temperature ranges were obtained to implant CNTs in the pore channels of the YSZ membranes without any defect. Of the two identified temperature ranges for the growth of CNTs, only at a temperature close to 750 °C could the protruding CNT grids be harvested. Filtration results showed that the presence of CNT grids greatly improves the removal of tiny emulsion particles from water in contrast to only YSZ pore channels alone. The YSZ membrane with CNT grids displayed 100% rejection rate to emulsion particles and retained a permeation flux of 0.6 L m^{-2} min^{-1} with a pressure drop of 1 atm over 3 days of operation. This performance was sustained by the formation of lipophilic soft layers on CNT grids, which has been proven by microscopic securitization. The lipophilic soft layers function as a lipo-rejection barrier exhibiting both adsorption and steric repulsion mechanisms jointly. The latter prevailed after the separation reached the steady state where both rejection and flux underwent negligible changing. The separation test also found desorption of oil molecules from the lipo-layer when the layer became thick enough. It is noteworthy that the widths of ceramic pore channels are also critical to the role of CNTs. Finally, the spent membrane can be regenerated through solvothermal treatment in an aprotic polar organic solvent.

AUTHOR INFORMATION

Corresponding Author

*Address: Department of Chemical and Biomolecular Engineering, National University of Singapore, 4 Engineering Drive 4, Blk E5, #02-22, Singapore 117576, Singapore. Tel.: +65 6516 5059. Fax: +65 6779 1936.

Notes

The authors declare no competing financial interest.

ACKNOWLEDGMENTS

This research was supported by National University of Singapore (NUS) and Singapore National Research Foundation (NRF) (Grant R279-000-261-281).

REFERENCES

(1) Mueller, J.; Cen, Y. W.; Davis, R. H. *J. Membr. Sci.* **1997**, *129*, 221−235.
(2) Basaran, T. K.; Demetriades, K.; McClements, D. J. *Colloids Surf., A* **1998**, *136*, 169−181.
(3) Yan, Y.; Masliyah, J. H. *Int. J. Multiphase Flow* **1993**, *19*, 875−886.
(4) Palaniandy, P.; Adlan, M. N.; Aziz, H. A.; Murshed, M. F. *Chem. Eng. J.* **2010**, *157*, 316−322.
(5) Santander, M.; Rodrigues, R. T.; Rubio, J. *Colloids Surf., A* **2011**, *375*, 237−244.
(6) Al-Shamrani, A. A.; James, A.; Xiao, H. *Colloids Surf., A* **2002**, *209*, 15−26.
(7) Zhao, X.; Wang, Y.; Ye, Z.; Borthwick, A. G. L.; Ni, J. *Process Biochem.* **2006**, *41*, 1475−1483.
(8) Ayotamuno, M. J.; Kogbara, R. B.; Ogaji, S. O. T.; Probert, S. D. *Appl. Energy* **2006**, *83*, 1258−1264.
(9) Rezvanpour, A.; Roostaazad, R.; Hesampour, M.; Nystrom, M.; Ghotbi, C. *J. Hazard. Mater.* **2009**, *161*, 1216−1224.
(10) Lin, S. H.; Lan, W. J. *Water Res.* **1998**, *32*, 2680−2688.
(11) Tansel, B.; Regula, J.; Shalewitz, R. *Water, Air, Soil Pollut.* **2001**, *126*, 291−305.
(12) Abbasi, M.; Mirfendereski, M.; Nikbakht, M.; Golshenas, M.; Mohammadi, T. *Desalination* **2010**, *259*, 169−178.
(13) Wang, L.; Wang, X.; Fukushi, K. i. *Desalination* **2008**, *229*, 181−191.

(14) Cui, J.; Zhang, X.; Liu, H.; Liu, S.; Yeung, K. L. *J. Membr. Sci.* **2008**, *325*, 420−426.
(15) Guizard, C.; Ayral, A.; Julbe, A. *Desalination* **2002**, *147*, 275−280.
(16) Lobo, A.; Cambiella, A.; Benito, J. M.; Pazos, C.; Coca, J. *J. Membr. Sci.* **2006**, *278*, 328−334.
(17) Nishio, M.; Hirota, M.; Umezawa, Y., *The CH/π Interaction: Evidence, Nature, And Consequences*; Wiley-VCH: New York, 1998; p 89.
(18) Pyrzynska, K. *Sep. Purif. Rev.* **2008**, *37*, 374−391.
(19) Joseph, L.; Zaib, Q.; Khan, I. A.; Berge, N. D.; Park, Y.-G.; Saleh, N. B.; Yoon, Y. *Water Res.* **2011**, *45*, 4056−4068.
(20) Upadhyayula, V. K. K.; Deng, S. G.; Mitchell, M. C.; Smith, G. B. *Sci. Total Environ.* **2009**, *408*, 1−13.
(21) Pan, B.; Xing, B. S. *Environ. Sci. Technol.* **2008**, *42*, 9005−9013.
(22) Lee, C. H.; Johnson, N.; Drelich, J.; Yap, Y. K. *Carbon* **2011**, *49*, 669−676.
(23) Lee, C.; Baik, S. *Carbon* **2010**, *48*, 2192−2197.
(24) Yu, M. F.; Lourie, O.; Dyer, M. J.; Moloni, K.; Kelly, T. F.; Ruoff, R. S. *Science* **2000**, *287*, 637−640.
(25) Demczyk, B. G.; Wang, Y. M.; Cumings, J.; Hetman, M.; Han, W.; Zettl, A.; Ritchie, R. O. *Mater. Sci. Eng., A* **2002**, *334*, 173−178.
(26) Baughman, R. H.; Zakhidov, A. A.; de Heer, W. A. *Science* **2002**, *297*, 787−792.
(27) Chen, X.; Hong, L.; Tai, X. H. *J. Am. Ceram. Soc.* **2011**, *94*, 382−390.
(28) Mattevi, C.; Wirth, C. T.; Hofmann, S.; Blume, R.; Cantoro, M.; Ducati, C.; Cepek, C.; Knop-Gericke, A.; Milne, S.; Castellarin-Cudia, C.; Dolafi, S.; Goldoni, A.; Schloegl, R.; Robertson, J. *J. Phys. Chem. C* **2008**, *112*, 12207−12213.
(29) Vermisogiou, E. C.; Pilatos, G.; Romanos, G. E.; Karanikolos, G. N.; Boukos, N.; Mertis, K.; Kakizis, N.; Kanellopoulos, N. K. *Microporous Mesoporous Mater.* **2008**, *110*, 25−36.
(30) Cains, P. W.; Martin, P. D.; Price, C. J. *Org. Process Res. Dev.* **1998**, *2*, 34−48.
(31) Piao, L. Y.; Li, Y. D.; Chen, J. L.; Chang, L.; Lin, J. Y. S. *Catal. Today* **2002**, *74*, 145−155.
(32) Fitch, R. M., *Polymer Colloids: A Comprehensive Introduction*, 1st ed.; Academic Press: San Diego, 1997; p 145.
(33) Hua, F. L.; Tsang, Y. F.; Wang, Y. J.; Chan, S. Y.; Chua, H.; Sin, S. N. *Chem. Eng. J.* **2007**, *128*, 169−175.
(34) Ohya, H.; Kim, J. J.; Chinen, A.; Aihara, M.; Semenova, S. I.; Negishi, Y.; Mori, O.; Yasuda, M. *J. Membr. Sci.* **1998**, *145*, 1−14.
(35) Yang, Y.; Chen, R.; Xing, W. *Sep. Purif. Technol.* **2011**, *76*, 373−377.
(36) Marchese, J.; Ochoa, N. A.; Pagliero, C.; Almandoz, C. *Environ. Sci. Technol.* **2000**, *34*, 2990−2996.
(37) Wandera, D.; Wickramasinghe, S. R.; Husson, S. M. *J. Membr. Sci.* **2011**, *373*, 178−188.